Full Length Research Paper

Experimental study of structural and optical band gap of nickel doped tin oxide nanoparticles

Mohsen Dehbashi[1]* and Mousa Aliahmad[2]*

Department of Physics, University of Sistan and Baluchestan, P. O. Box 98135-674, Zahedan, Iran.

Nickel-doped tin oxide nanoparticles were synthesized by a simple co-precipitation method. The structural, morphological and optical properties of these nanoparticles were investigated using X-ray diffraction, transmission electron microscopy and UV-Vis spectroscopy. The X-ray diffraction revealed that all samples are pure rutile-type tetragonal phase; and the nickel doping did not change the tetragonal structure of tin oxide but the grain crystalline size decreased to 27 and 23 nm for Ni doping of 1 and 2 wt%, respectively. The effective strain values of the samples increased with increasing amounts of doping Ni. The TEM image confirmed that the size of nickel-doped tin oxide particles is in the range of nanoscale materials. UV-Vis spectroscopy has revealed the optical band gap to be 4.06, 4.08 and 4.10 eV for pure and Ni (1 and 2 wt.%) doped SnO_2 nanoparticles, respectively.

Key words: Nanoparticles, nickel-doped, tin oxide, tetragonal, band gap.

INTRODUCTION

Tin oxide is an important material due to its properties such as high degree of transparency in the visible spectrum, strong physical and chemical interaction with adsorbed species, low operating temperature and strong thermal stability in air (up to 500°C) (Zhu et al., 2006). It is an n-type semiconductor with a large band gap (3.6 eV at the room temperature), which can be used in gas sensors, solar cells, glass electrodes and secondary lithium batteries (Morales and Sanchez, 1999; Wang and Lee, 2003; Warnken et al., 2001; Nayral et al., 2000). A number of attempts have been made by developing effective synthetic techniques in the preparation of metal ions-doped SnO_2 nanoparticles, such as sol–gel (Lincoln et al., 2004), co-precipitation (Rumyantseva et al., 2005) and chemical vapor deposition (Wang et al., 2005). In this work, we synthesize Ni-doped SnO_2 nanoparticles by chemical co-precipitation method because this method has some advantages such as precise control over the stoichiometry, low temperature synthesis, high purity and high chemical homogeneity.

EXPERIMENTAL

Ni-SnO_2 nano-powders were successfully prepared by means of dissolving tin chloride (hydrous $SnCl_2.2H_2O$ (98% Merck)) and nickel chloride (hydrous $NiCl_2\cdot6H_2O$ (98% Merck)) in double distilled water, this was followed by the addition of sufficient amount of aqueous ammonia to the above solution which was then stirred for 2 h. The dropping rate must be control properly for the chemical homogeneity. The precipitate was washed with double distilled water for many times. Then it dried at 100°C for several hours. Heating treatment of the synthesized nanoparticles was conducted in air for 2 h at 350°C.

Crystallinity, structure and particle size of Ni-doped SnO_2 nanoparticles were determined by X-ray diffraction (XRD) using Rigaku-Miniflex X-ray diffractometer with CuKα radiations (λ=0.15406 nm) in 2θ range from 10° to 70°. Morphology and particle size obtained with a Hitachi H-800 transmission electron microscope (TEM) and UV-Vis transmittance spectra of the samples were recorded at room temperature by using PG instrument T80 UV-Vis spectrophotometer.

RESULTS AND DISCUSSION

XRD patterns of $Sn_{1-x}Ni_xO_2$ (with x = 0.01 and 0.02) annealed at 350°C for 2 h are shown in Figure 1, in which (a), (b) and (c) correspond to x = 0.01 and 0.02, respectively.

---

*Corresponding author. E-mail: physicm@yahoo.com, aliahmad@phys.usb.ac.ir. Tel/Fax: +985412446565.
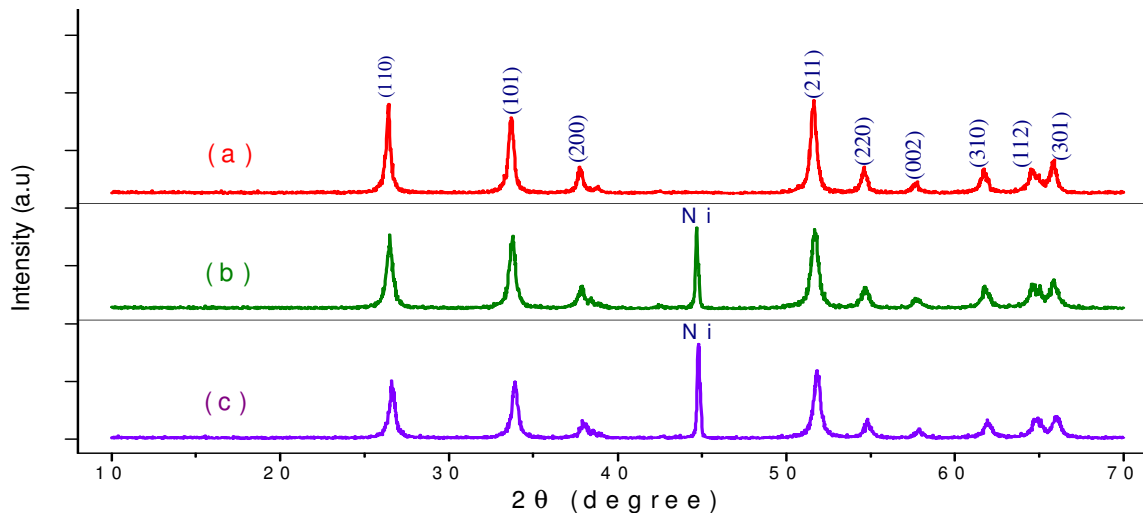
Figure 1. XRD patterns of (a) SnO_2, (b) $Sn_{0.99}Ni_{0.01}O_2$ and (c) $Sn_{0.98}Ni_{0.02}O_2$ nanoparticles.

Table 1. Structural parameters of samples in different Ni content and their optical band gap.

Sample	Ni (wt.%)	D_{110} (nm)	a (A˚)	c (A˚)	Δa (A˚)	Δc (A˚)	Volume of unit cell (A˚³)	No. of unit cells in the one particle	Optical band gap E_g (eV)
SnO_2	0	31	4.765	3.200	0.027	0.012	72.66	205×10^3	4.06
$Sn_{0.99}Ni_{0.01}O_2$	1	27	4.751	3.193	0.013	0.005	72.08	138×10^3	4.08
$Sn_{0.98}Ni_{0.02}O_2$	2	23	4.733	3.183	-0.005	-0.005	71.31	89×10^3	4.10

All diffraction peaks are well assigned to tetragonal crystalline phase of tin oxide (with the reference pattern JCPDS 880287), and the Ni doping does not change the tetragonal structure of SnO_2. From Figure 1, it is noted that the intensity of the $Sn_{1-x}Ni_xO_2$ peaks decreases with increasing Ni content and the full-width at half-maximum (FWHM) widths of the peaks increases with increasing Ni content, as well indicates that crystalline size of the $Sn_{1-x}Ni_xO_2$ powders decreases gradually as the Ni content increases. The crystalline size of samples are calculated using Scherrer's formula,

$$D_{hkl} = \frac{0.9\lambda}{\beta_{hkl}\cos(\theta)}$$

(1)

Where λ is the wavelength of CuKα radiation ($\lambda=$ 0.154056 nm), is the full width at half maximum (FWHM) of the *(hkl)* peak at the diffracting angle $2\theta_{hkl}$ (Patterson, 1939), the (110) peak is used to calculate the crystalline sizes.

The crystalline size of samples were found to be 31, 27, and 23 nm corresponding to SnO_2, $Sn_{0.99}Ni_{0.01}O_2$ and $Sn_{0.98}Ni_{0.02}O_2$ samples respectively using scherrer's formula. For the tetragonal structure, the lattice constants can be calculate from:

$$\frac{1}{d_{hkl}^2} = \frac{h^2 + k^2}{a^2} + \frac{l^2}{c^2}$$

(2)

and

$$2d_{hkl}\sin(\theta) = m\lambda$$

(3)

Where *h*, *k*, and *l* are all integers, *(hkl)* is the lattice plane index, *a* and *c* are lattice constants, d_{hkl} is distance between two consecutive planes (m=1) with lattice plane index *(hkl)*. Structural parameters of samples in different Ni content are presented in Table 1, in which *a* and *c* are calculated from XRD peaks (110) and (101), Δa and Δc are the differences between the measured lattice constant and that of the bulk SnO_2 for *a* = 4.738 A˚ and *c* = 3.188 A˚ respectively. Effect of nickel content on the lattice constants are shown in Figure 2. In addition, the effective particle size *δ* and the effective strain *η* are related by the following equation (Williamson and Hall, 1953):

$$\frac{\beta\cos(\theta)}{\lambda} = \frac{0.9}{\delta} + \eta\frac{\sin(\theta)}{\lambda}$$

(4)
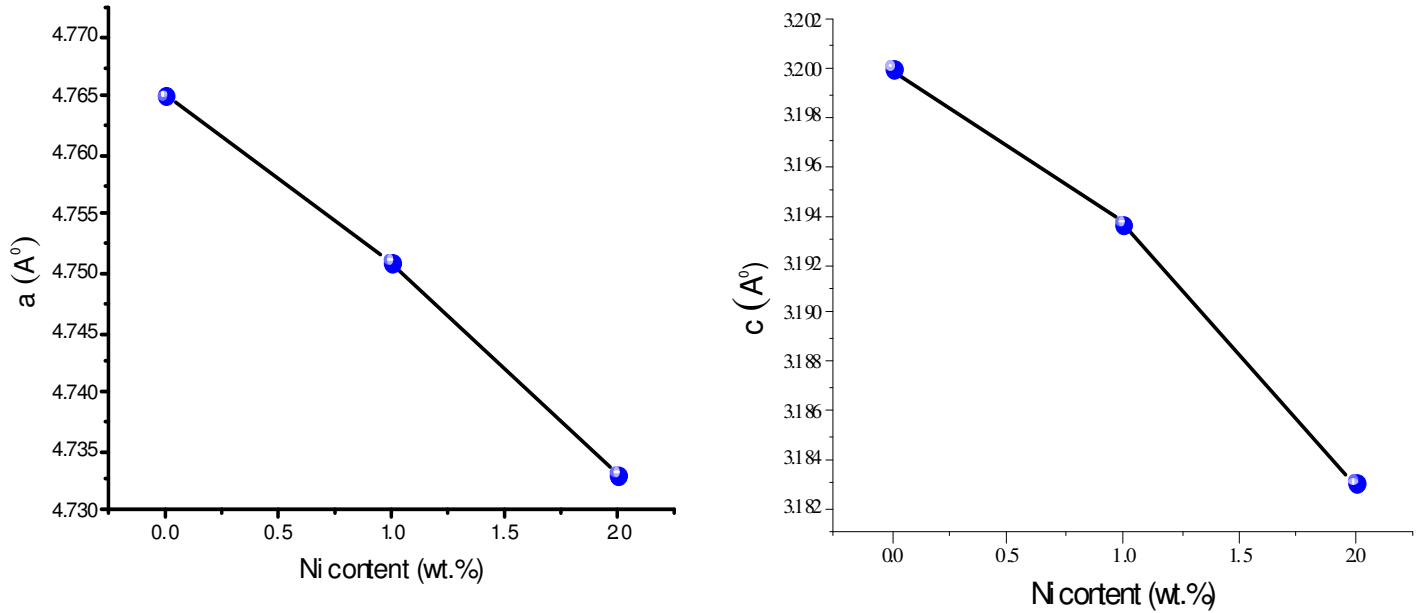
Figure 2. Effect of nickel content on the lattice constants (a and c).
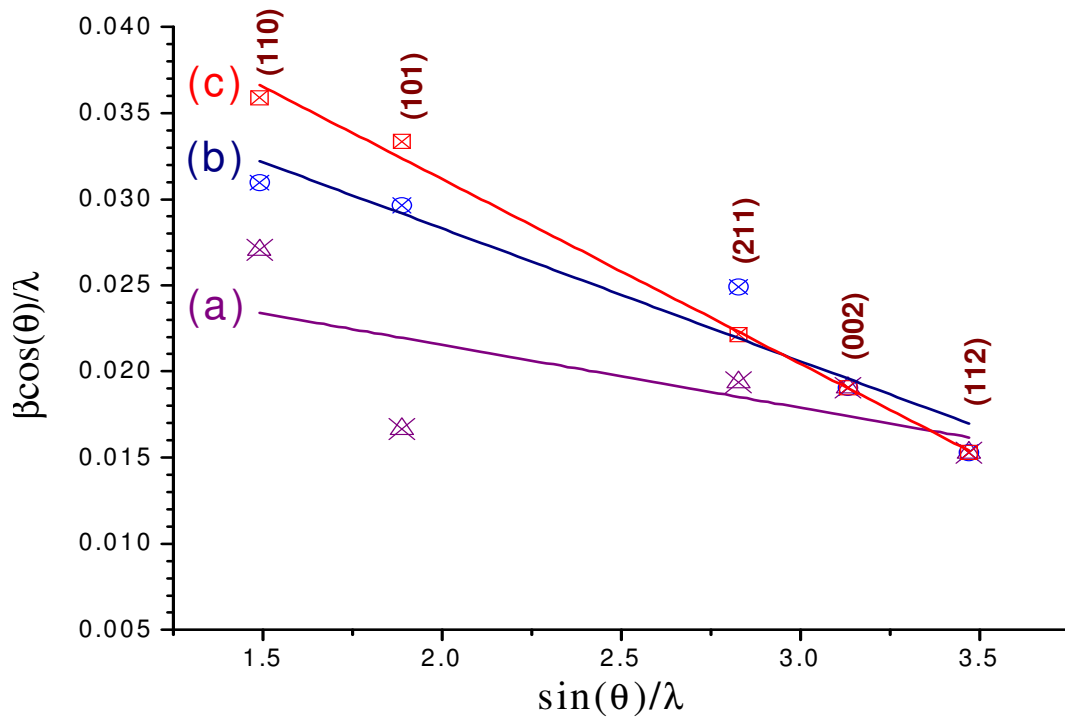
Figure 3. Williamson–Hall plot of (a) SnO_2, (b) $Sn_{0.99}Ni_{0.01}O_2$ and (c) $Sn_{0.98}Ni_{0.02}O_2$ samples and corresponding linear fits using equation 4.

Figure 3 represents the plot of $\beta cos(\theta)/\lambda$ against $sin(\theta)/\lambda$. Slope of the graph depicts effective strain that values vary from -3.65×10^{-3} to -1.07×10^{-2} as the nickel content increases. Moreover, the intercept on y-axis gives $0.9/\delta$ and therefore the effective particle size that lie in the range of 23 to 37 nm. It is clear from the effective strain results that as the Ni content increases, the effective strain value increases (Figure 4).
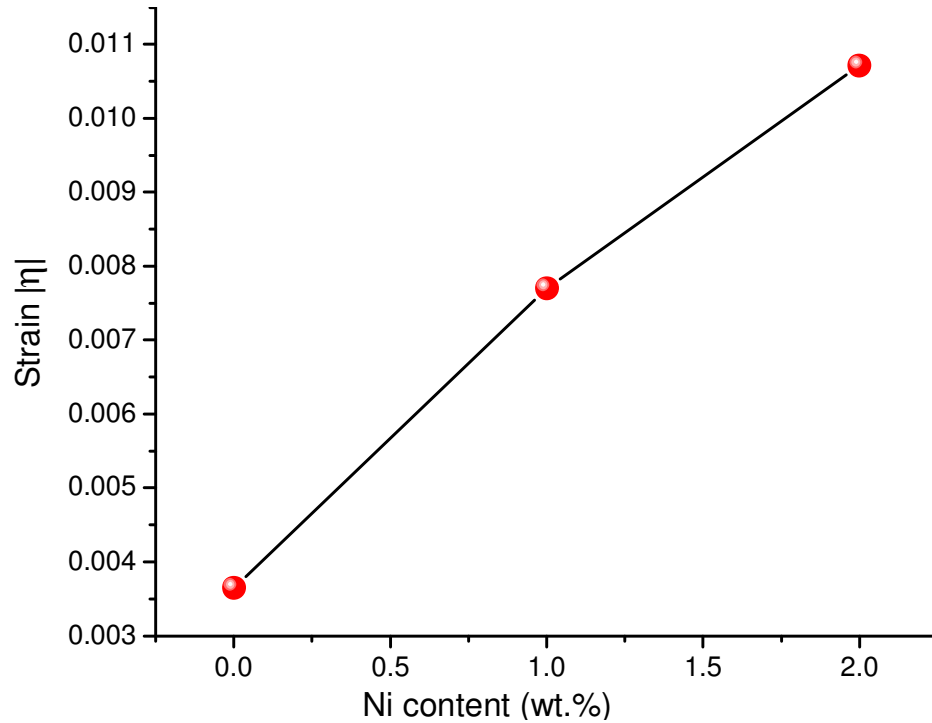
Figure 4. Variation of effective strain with Ni content.
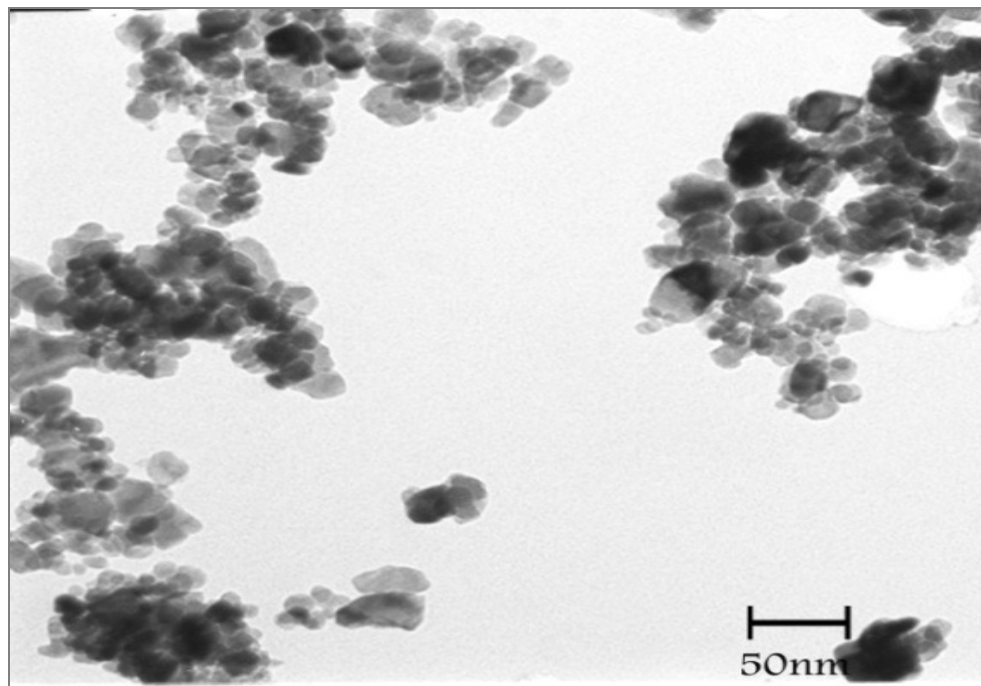
Figure 5. TEM image of $Sn_{0.99}Ni_{0.01}O_2$ nanoparticles.

Figure 5 illustrates the TEM image of $Sn_{0.99}Ni_{0.01}O_2$ nanoparticles calcined at 350°C for 2 h, it is shown that the powder are not well uniform in size and part of the particles are found to be agglomerated. In general, agglomeration occurs in the case of nanoparticles very easily because the surface forces such as Vander-Waals
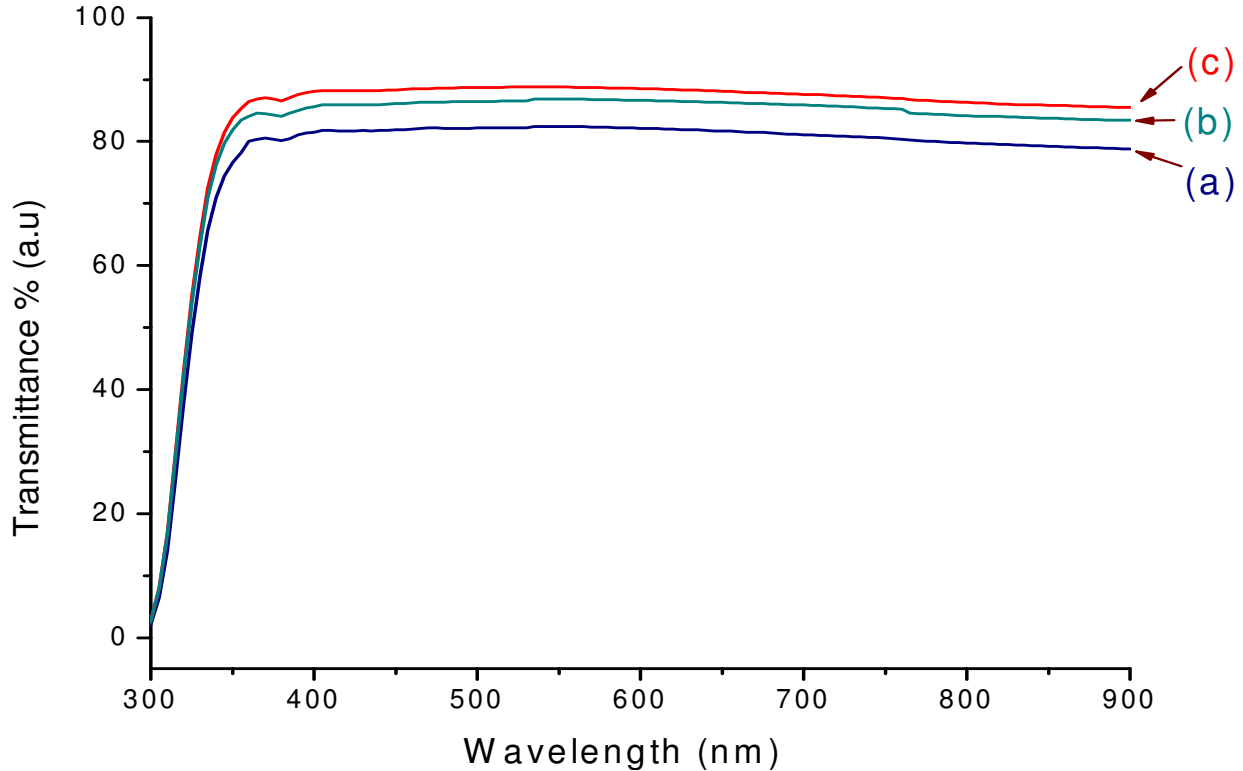
Figure 6. Transmittance spectra for the (a) SnO_2, (b) $Sn_{0.99}Ni_{0.01}O_2$ and (c) $Sn_{0.98}Ni_{0.02}O_2$ nanoparticles.

forces, capillary forces and electrostatic forces could overcome only against gravitational and inertial forces for particles in this size range (Pugh and Bergstro, 1994). The average diameters of particles for proper dispersed regime were evaluated to be less than 50 nm. Grain particle size was obtained by using Scherrer's formula from XRD calculation and the particle size obtained from TEM image for monodispersed part are close to each other approximately.

Figure 6 shows optical transmittance spectra of the samples (a), (b) and (c). The samples are transparent in a large range of wavelength (bigger 350 nm). In order to calculate the optical band gap we used the Tauc relation,

$$\alpha h\nu = B(h\nu - E_g)^n \tag{5}$$

Where α is the absorption coefficient, B is a constant, $h\nu$ energy of incident photons and Exponent n depends on the type of the transition, n may have values 1/2, 2, 3/2 and 3 corresponding to the allowed direct, allowed indirect, forbidden direct and forbidden indirect transitions respectively (Pankove, 1971).

Since α and transmittance (T) are correlated as,

$$T = \exp(-\alpha L) \tag{6}$$

or

$$\alpha = -\frac{(\ln T)}{L} \tag{7}$$

Where L is the thickness of the sample, for direct allowed transition ($n=1/2$) we have,

$$(h\nu \ln T)^2 = B^2 L^2 (h\nu - E_g) \tag{8}$$

The exact value of the optical band gap is determined by extrapolating the straight-line portion of $(h\nu \ln T)^2$ vs. $h\nu$ graph to the $h\nu$ axis (Figure 7). The values of the optical band gap at the different Ni content are shown in Table 1. The optical band gap values are higher than the bulk value of SnO_2 (3.6 eV at the room temperature), the optical band gap is found to be particle size dependent and increases with increasing Ni content or it is increasing with decreasing particle size.

Conclusion

Ni doped SnO_2 nanoparticles have been successfully synthesized using simple co-precipitation method. Crystalline size of particles are in range of 23 to 31 nm, it is shown that the crystalline size of the nanoparticles decreases with increasing amounts of doping Ni, and nanoparticles have pure rutile structure. TEM image of $Sn_{0.99}Ni_{0.01}O_2$ nanoparticles shows that the powders
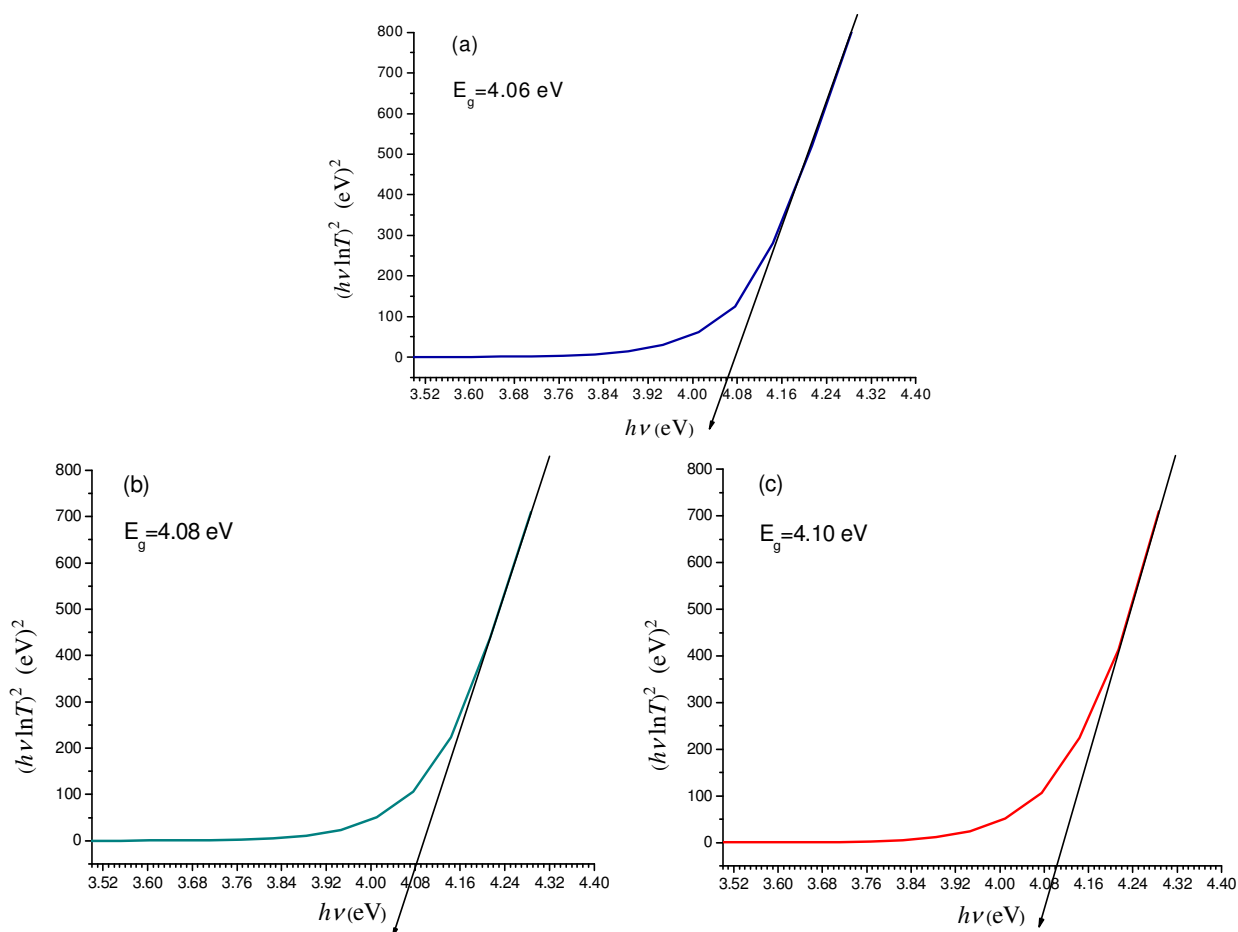
Figure 1. Determination of optical band gap from the transmittance spectra for the (a) SnO_2, (b) $Sn_{0.99}Ni_{0.01}O_2$ and (c) $Sn_{0.98}Ni_{0.02}O_2$ nanoparticles.

contain a good size distribution. Apart from the agglomeration regime in the TEM image, the particle size of the sample is less than 50 nm. Transmittance spectra of samples show that the optical band gap values of samples are higher than the bulk value of SnO_2; this is because of nanosize particles. In this range of nanosize particles (23 to 31 nm), the optical band gap change is very small.

REFERENCES

Lincoln AK, Sergio TF, Ren´ı VSA, Yoshitak G, Antonio ASA, Sandra Cde C (2004). Copper (II) adsorbed on SiO_2/SnO_2 obtained by the sol–gel processing method: application as electrochemical sensor for ascorbic acid. J. Colloid Interface Sci. 274:579.

Morales J, Sanchez L (1999). Electrochemical behaviour of SnO_2 doped with boron and indium in anodes for lithium secondary batteries. Solid State Ionics. ScienceDirect. 126:219.

Nayral C, Viala E, Fau P, Senocq F, Jumas J C, Maisonnat A, Chaudret B (2000). Synthesis of Tin and Tin oxide nanoparticles of low size dispersity for application in gas sensing. Chem. A Eur. J. 6:4082.

Patterson AL (1939). The Scherrer formula for x-ray particle size determination. Phys. Rev. Online Arch. (Prola) 56:978–982.

Pugh RJ, Bergstrom L (1994). Surface and colloid chemistry in advanced ceramic processing. Marcel Dekker, New York, 273.

Rumyantseva MN, Kovalenko VV, Gaskov A M, Pagnier T, Machon D, Arbiol J, Morante JR (2005). Nanocomposites SnO_2/Fe_2O_3: Wet chemical synthesis and nanostructure characterization. Sens. Actuators B 109:64.

Tauc J, Menth A (1972). States in the gap. Non Cryst. Solids 8:569.

Wang JX, Chen HY, Gao Y, Liu DF, Song L, Zhang ZX, Zhao XW, Dou XY, Luo SD, Zhou WY, Wang G, Xie SS (2005). Synthesis and characterization of In_2O_3/SnO_2 hetero-junction beaded nanowires. J. Cryst. Growth 284:73.

Wang Y, Lee JY (2003). Preparation of SnO_2–graphite nanocomposite anodes by urea-mediated hydrolysis. Electrochem. Commun. 5:292.

Warnken M, Lazark K, Wark M (2001). Redox behaviour of SnO_2 nanoparticles encapsulated in the pores of zeolites towards reductive gas atmospheres studied by in situ diffuse reflectance UV/Vis and Mössbauer spectroscopy. Phys. Chem. Chem. Phys. 3:1870.

Williamson GK, Hall WH (1953). X-ray line broadening from filed aluminium and wolfram. Acta Metall. pp. 22–31.

Zhu J, Tay B Y, Ma J (2006). Synthesis of mesoporous tin oxide on neutral surfactant templates. Mater. Lett. 60:1003.